Efficient Free-Surface Kirchhoff Modeling

Lúcio Santos
William Symes

CRPC-TR95556
August 1995

Efficient Free–Surface Kirchhoff Modeling

Lúcio T. Santos *

William W. Symes †

August 7, 1995

Abstract

The aim of this work is to introduce a new scheme to apply Kirchhoff modeling efficiently to a 2-D acoustic model with a free surface and with irregular source and receiver locations. We consider as data all the traveltimes and amplitudes of each ray connecting points below some datum depth and points over this depth. We derive a new expression for the Kirchhoff formula which uses these computed traveltimes and amplitudes only. Given accurate components, the primary reflection seismograms computed via this new approach for the Kirchhoff method is remarkably accurate and less expensive than the usual technique. We also compare Kirchhoff seismograms with those produced from the same model by finite-difference solution of the linearized acoustic wave equation.

Keywords: Kirchhoff modeling, High frequency approximations.

AMS Subject Classification: 78A05, 86A15.

---

*Dept. of Applied Mathematics, State University of Campinas, CP 6065, 13081-970 Campinas (SP), Brazil (lucio@ime.unicamp.br), and visiting member of the Center for Research on Parallel Computation and the Department of Computational and Applied Mathematics, Rice University, Houston, TX 77251-1892, USA (lucio@rice.edu).

†Dept. of Computational and Applied Mathematics, Rice University, PO BOX 1892, Houston, TX 77251-1892, USA (symes@rice.edu)

1   Introduction

Imaging methods based on high frequency asymptotic approximations of the acoustic Green's function, sometimes called *Kirchhoff modeling*, are an efficient tool for computing primaries only reflection seismograms ([3], [4]). Their popularity relies on the fact that they can produce a seismogram for a fixed time window, using a portion of the avaliable data only, and with a smaller cost than the others classical techniques such as finite–difference solution of the full acoustic wave equation (e.g. [1], [5]). We will discuss Kirchhoff modeling explicitly, but the same considerations apply to high–frequency asymptotic inversion algorithms as well.

The straightforword Kirchhoff modeling requires the tabulation of the traveltimes and amplitudes for each ray connecting the source and the receiver with the points in the region under consideration. Therefore, we must compute two traveltime and amplitude tables. For models consisting of an acoustic medium with constant density, and a free surface at $z = 0$, the image principle states that if z_p is the source or receiver depth then the free–surface Green's function $G_F(z_p)$ can be written as

$$G_F(z_p) = G(z_p) - G(-z_p) \, , \tag{1}$$

where $G(z_p)$ is the free–space Green's function with the velocity field evenly extended about $z = 0$. Since the Kirchhoff algorithm requires the traveltime and amplitude tables not only for source positions but also for receiver positions, to simulate the free–surface model we must compute four related tables: two for the true positions, z_s and z_r, and two for the "ghost" positions, $-z_s$ and $-z_r$, which can be very expensive.

In order to reduce the cost of such computations, for z_p close enough to the surface ($z_p \approx 0$), from Taylor's expansion the following approximation to (1) can be used

$$G_F(z_p) \approx 2 \, z_p \, \left. \frac{d}{dz_p} G(z_p) \right|_{z_p=0} . \tag{2}$$

However, a very naive computation using the homogeneous Green's function in frequency domain indicates that to achieve a reasonable accuracy for the above approximation, z_p must be at most a fraction of a wavelength away from the free surface. Figure 1 shows

the average of the relative errors in the L_2–norm for approximation (2) as a function of the number of wavelengths for z_p. For instance, for $z_p = 0.2$ wavelengths the relative error is about 8% and for $z_p = 0.4$ wavelengths it is 43%. It is interesting to observe how fast the error increases as z_p becomes greater. As a result, since in practical experiments z_p maybe close to half a wavelength, the approximation (2) is not very accurate, and then we need to compute the four traveltime/amplitude tables.
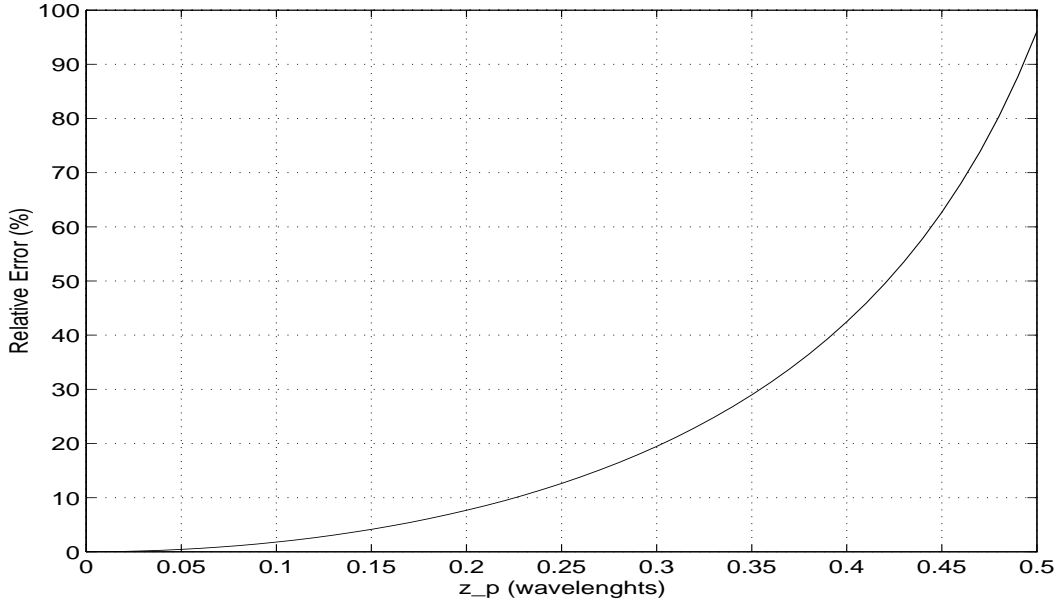

Figure 1: Relative error in the L_2–norm for the approximation of the free–surface Green's funtion: $G_F(z_p) = G(z_p) - G(-z_p) \approx 2z_p \left. \dfrac{dG(z_p)}{dz_p} \right|_{z_p=0}$.

The objective of this work is to introduce a different scheme for applying the Kirchhoff algorithm to free–surface models, with computational cost only slightly higher than from that of free–space Kirchhoff modeling. We consider as data all the traveltimes and amplitudes of each ray connecting points below some datum depth z_d and points over the line $z = z_d$. With a formula relating that data to the solution for any pair source–receiver above the datum depth, we derive a new approximate expression for the Kirchhoff formula, using traveltimes and amplitudes at the datum depth only.

Denoting by N_s the number of source positions, by N_r the number of receiver positions

for each shot, and by N_d the number of points on the datum depth, the free–space Kirchhoff algorithm will require the computation of $N_s N_r$ traveltime and amplitude tables in general (i.e. if the placement of sources and receivers is arbitrary) whereas in our approach only N_d tables are needed. For the free–surface case the comparison is between $2 N_s N_r$ and N_d. If we assume that the source and receiver positions are regularly spaced at the same depth and overlap, the number of traveltime and amplitude tables needed is at most $N_s + N_r$ in the free–space case and $2 N_s + 2 N_r$ in the free–surface case. Therefore, provided the sources and receivers are spaced densely enough so that $N_d \approx N_s + N_r$, our new scheme is less expensive than the obvious technique, for both free–space and free–surface models, and much less so for irregular source/receiver positions.

Given accurate components, the primary reflection seismograms computed via this new approach for the Kirchhoff method is remarkably accurate, for models within its domain of validity. We illustrate the accuracy of the Kirchhoff seismograms by comparing them with those produced from the same model by a finite–difference code.

This paper is organized as follows. In Section 2 we present some Green's functions which are necessary to the development of the work. In Section 3 we devise the formula relating the free–space solution at the datum depth to the required solution for any pair source–receiver. We also develop some asymptotic approximations. In Section 4 we describe the implementation of the new scheme for the free–surface Kirchhoff modeling. In Section 5 we show numerical examples that illustrate the validity of our approach, and the inaccuracy of the derivative approximation for the free–surface Green's function. Finally, in Section 6 we present our conclusions concerning practical computations.

2   Green's Functions

Our 2-D model consists of an isotropic acoustic medium with constant density, bounded above by a free surface at $z = 0$ (the z-axis points downwards). The datum depth is at $z = z_d > 0$ and the medium between $z = 0$ and $z = z_d$ is homogeneous of constant velocity v_0 (see Figure 2). This applies directly to marine problems. The rapidly varying part of the velocity field ($r(x, z) \equiv$ *reflected field*) is treated as a first order perturbation of the slowly

varying part $(v(x,z) \equiv velocity\ field)$. We have $v_{total}(x,z) = v(x,z)[1 + r(x,z)]$, that is, r is the oscilllatory relative perturbation of the smooth velocity v and it is dimensionless.
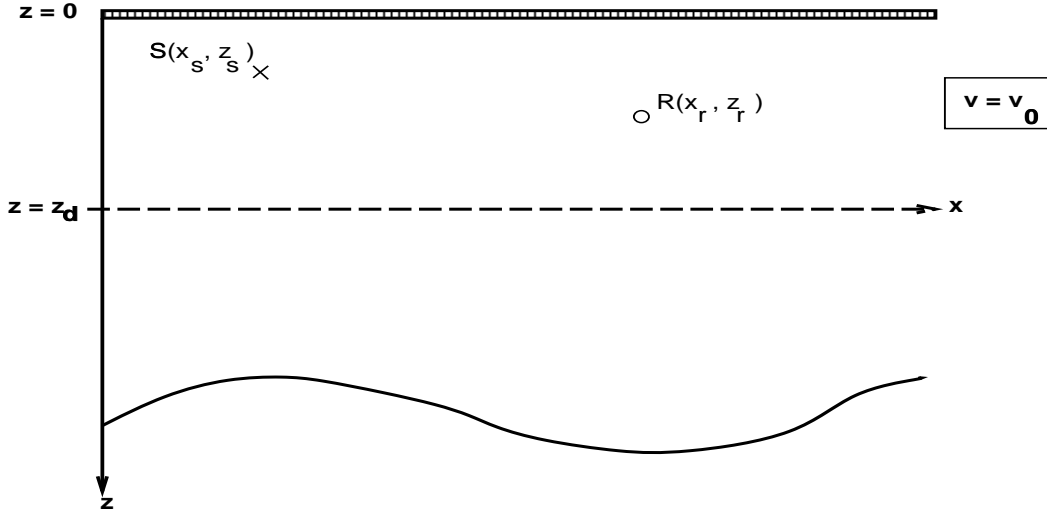

Figure 2: Free–surface model. The medium between the free surface and the datum depth is homogeneous.

We also assume that there are no turning rays: incident rays are entirely downgoing (or upcoming, depending on the relative positions of source and receiver), and reflected rays are entirely upcoming (respectively, downgoing), at least for the time window under consideration. The discussion to follow will develop relations amongst four Green's functions for the wave equation with various coefficients and boundary conditions.

The inhomogeneous free–surface Green's function $G_F(x,z,t;\overline{x},\overline{z})$ satisfies the equations

$$\begin{cases} \left(\dfrac{1}{v(x,z)^2} \dfrac{\partial^2}{\partial t^2} - \nabla^2 \right) G_F(x,z,t;\overline{x},\overline{z}) = \delta(t)\delta(x - \overline{x})\delta(z - \overline{z}) \\ G_F(x,0,t;\overline{x},\overline{z}) = 0 \\ G_F(x,z,t;\overline{x},\overline{z}) \equiv 0\ ,\ t < 0 \end{cases}$$

We denote by $G(x,z,t;\overline{x},\overline{z})$ the inhomogeneous free–space Green's function with

$v(x, z) = v(x, -z)$ for $z < 0$, that is, the solution of

$$\begin{cases} \left(\dfrac{1}{v(x,z)^2} \dfrac{\partial^2}{\partial t^2} - \nabla^2 \right) G(x, z, t; \overline{x}, \overline{z}) = \delta(t)\delta(x - \overline{x})\delta(z - \overline{z}) \\[2mm] G(x, z, t; \overline{x}, \overline{z}) \equiv 0 \ , \ t < 0 \end{cases} \tag{3}$$

It is a well known result that by the image principle (cf. [7]) G_F can be written as

$$G_F(x, z, t; \overline{x}, \overline{z}) = G(x, z, t; \overline{x}, \overline{z}) - G(x, z, t; \overline{x}, -\overline{z}) \ , \tag{4}$$

that is, G_F is the difference between two free–space Green's functions for two different source positions: $(\overline{x}, \overline{z})$ and $(\overline{x}, -\overline{z})$.

Let $G_H(x, z, t; \overline{x}, \overline{z})$ be the homogeneous free–space Green's function given by the solution of equation (3) with $v(x, z) \equiv v_0$. Recall that G_H is expressed as (see [2])

$$G_H(x, z, t; \overline{x}, \overline{z}) = \frac{H(t - R/v_0)}{2\pi \sqrt{t^2 - (R/v_0)^2}} \ , \tag{5}$$

where $R = \sqrt{(x - \overline{x})^2 + (z - \overline{z})^2}$ and $H(.)$ is the Heaviside function.

Let us now define a new velocity field for the whole medium by $v_N(x, z) = v(x, z)$ for $z \geq z_d$ and $v_N(x, z) = v(x, 2z_d - z)$ for $z \leq z_d$, i.e. v_N is a evenly extension of v about $z = z_d$. We introduce the Green's function $G_N(x, z, t; \overline{x}, \overline{z})$ as the solution of

$$\begin{cases} \left(\dfrac{1}{v_N(x,z)^2} \dfrac{\partial^2}{\partial t^2} - \nabla^2 \right) G_N(x, z, t; \overline{x}, \overline{z}) = \delta(t)\delta(x - \overline{x})\delta(z - \overline{z}) \\[3mm] \hspace{4cm} + \ \delta(t)\delta(x - \overline{x})\delta(z - 2z_d + \overline{z}) \\[3mm] G_N(x, z, t; \overline{x}, \overline{z}) \equiv 0 \ , \ t < 0 \end{cases} \tag{6}$$

It can be easily shown that the following property holds for G_N:

P1. $\left. \dfrac{\partial}{\partial z} G_N(x, z, t; \overline{x}, \overline{z}) \right|_{z=z_d} = 0$.

Moreover, since we are avoiding the possibility of turning rays, G_N also satisfies for $\overline{z} > z_d$

P2. $G_N(x, z_d, t; \overline{x}, \overline{z}) = 2\, G(x, z_d, t; \overline{x}, \overline{z})$.

These properties will be necessary in the next section to derive a useful formula for computing the Green's function G, knowing all its values on the datum depth $z = z_d$.

3   Computation of G using the data at $z = z_d$

3.1   Exact Solution

By applying Green's identity to $G(x, z, t; \tilde{x}, \tilde{z})$ (equation (3) with $\tilde{z} \leq z_d$) and $G_N(x, z, t' - t; x', z')$ (equation (6) with $z' \geq z_d$ and $t' \geq 0$) and taking the domain of integration to be the lower half–plane bounded above by $z = z_d$, we have

$$\int_{-\infty}^{\infty} dt \int_{-\infty}^{\infty} dx \int_{z_d}^{\infty} dz \left[G \nabla^2 G_N - G_N \nabla^2 G \right] =$$
$$\int_{-\infty}^{\infty} dt \int_{-\infty}^{\infty} dx \left[G_N \frac{\partial G}{\partial z} - G \frac{\partial G_N}{\partial z} \right]_{z=z_d} .$$

Using properties (P1) and (P2), we find

$$G(x', z', t'; \tilde{x}, \tilde{z}) = -2 \int_0^{t'} dt \int_{-\infty}^{\infty} dx \, G(x, z_d, t' - t; x', z') \cdot \left. \frac{\partial}{\partial z} G(x, z, t; \tilde{x}, \tilde{z}) \right|_{z=z_d} ,$$

or equivalently,

$$G(x', z', t'; \tilde{x}, \tilde{z}) = -2 \int_{-\infty}^{\infty} dx \, G(x, z_d, t'; x', z') * \left. \frac{\partial}{\partial z} G(x, z, t'; \tilde{x}, \tilde{z}) \right|_{z=z_d} , \qquad (7)$$

where $*$ denotes convolution in time.

Now, since the ray connecting $(\tilde{x}, \tilde{z})$ and (x, z_d) is entirely downgoing (as assumed in the previous section), we can make the following approximation

$$\left. \frac{\partial}{\partial z} G(x, z, t; \tilde{x}, \tilde{z}) \right|_{z=z_d} \approx \left. \frac{\partial}{\partial z} G_H(x, z, t; \tilde{x}, \tilde{z}) \right|_{z=zd} \equiv \frac{\partial}{\partial z_d} G_H(x, z_d, t; \tilde{x}, \tilde{z}) ,$$

and so, equation (7) can be approximated by

$$G(x', z', t'; \tilde{x}, \tilde{z}) \approx -2 \int_{-\infty}^{\infty} dx \, G(x, z_d, t'; x', z') * \frac{\partial}{\partial z_d} G_H(x, z_d, t'; \tilde{x}, \tilde{z}) . \qquad (8)$$

Expression (8) gives the free–space Green's function for any pair (x', z')–$(\tilde{x}, \tilde{z})$ in terms of its known values at the datum depth z_d and the normal derivative of the corresponding solution in homogeneous medium.

3.2   Asymptotic Solution

In this section we present an asymptotic approximation to equation (8) in order to establish a suitable relation for numerical computation. We begin by making the following

approximation for $t \approx \tau$,

$$\frac{H(t-\tau)}{2\pi\sqrt{t^2-\tau^2}} \approx \frac{H(t-\tau)}{2\pi\sqrt{2\tau}\sqrt{t-\tau}} = \frac{\mu(t-\tau)}{2\pi\sqrt{2\tau}} \, ,$$

where $\mu(t) = t^{-1/2} H(t)$. Therefore, $G_H(x,z,t;\tilde{x},\tilde{z})$ given by equation (5), can be approximated by

$$G_H(x,z,t;\tilde{x},\tilde{z}) \approx \frac{\mu(t-R/v_0)}{2\pi\sqrt{2R/v_0}} \, , \tag{9}$$

with $R = \sqrt{(x-\tilde{x})^2 + (z-\tilde{z})^2}$.

A similar approximation is valid for $G(x,z,t;x',z')$, that is,

$$G(x,z,t;x',z') \approx a(x,z;x',z') \, \mu(t-\tau(x,z;x',z')) \, , \tag{10}$$

where $a(x,z;x',z')$ and $\tau(x,z;x',z')$ can be calculated, for instance, by proper finite–difference codes (e.g. [6], [8], [9]).

In order to make the notation more compact, we write $a(x) \equiv a(x,z_d;x',z')$, $\tau(x) \equiv \tau(x,z_d;x',z')$ and $R(x) \equiv \sqrt{(x-\tilde{x})^2 + (z_d-\tilde{z})^2}$.

Substituing (9) and (10) in (8) we find,

$$G(x',z',t';\tilde{x},\tilde{z}) \approx -2 \int_{-\infty}^{\infty} dx \, a(x) \, \mu(t'-\tau(x)) \, * \, \frac{\partial}{\partial z_d} \left[\frac{\mu(t'-R(x)/v_0)}{2\pi\sqrt{2R(x)/v_0}} \right] \, . \tag{11}$$

Using the fact that $\dfrac{\partial R}{\partial z_d} = -\dfrac{\partial R}{\partial \tilde{z}}$ and $\mu(t-a) * \mu(t-b) = \pi H(t-a-b)$, equation (11) takes the form

$$G(x',z',t';\tilde{x},\tilde{z}) \approx \sqrt{\frac{v_0}{2}} \int_{-\infty}^{\infty} dx \, a(x) \frac{\partial}{\partial \tilde{z}} \left[\frac{H(t'-\tau(x)-R(x)/v_0)}{\sqrt{R(x)}} \right] \, . \tag{12}$$

Now, we assume that the major contribution of the $\tilde{z}$-derivative to the above integral is given by the term $\dfrac{z_d-\tilde{z}}{v_0 R(x)^{3/2}} \delta(t'-\tau(x)-R(x)/v_0)$. Such assumption has the flavour of the hypothesis made when high frequency approaches are used. Hence, equation (12) becomes

$$G(x',z',t';\tilde{x},\tilde{z}) \approx \frac{1}{\sqrt{2v_0}} \int_{-\infty}^{\infty} dx \, a(x) \frac{z_d-\tilde{z}}{R(x)^{3/2}} \delta(t'-\tau(x)-R(x)/v_0) \, .$$

Let α be the unique minimizer of the function $T(x) = \tau(x) + R(x)/v_0$, that is, $T'(\alpha) = 0$ and $\beta \equiv T''(\alpha) > 0$, where the prime indicates derivative with respect to x.

Therefore, expanding T in a second order Taylor's series around $x = \alpha$, and denoting $\tilde{t} = T(\alpha)$, we have

$$T(x) \approx \tilde{t} + \frac{\beta}{2}(x - \alpha)^2 \ .$$

Making the variable transform $\gamma = T(x)$ and after some algebraic manipulation in the above integral, we finally find

$$G(x', z', t'; \tilde{x}, \tilde{z}) \approx \frac{(z_d - \tilde{z}) \ a(\alpha)}{\sqrt{v_0 \ \beta} \ R(\alpha)^{3/2}} \mu(t' - \tilde{t}) \ . \tag{13}$$

It is worthwhile comparing the expression for the Green's function in both homogeneous and inhomogeneous cases, given by equations (9) and (13), respectively. The asymptotic approximation (13) can also be achieved by applying the stationary–phase method (see [2]) to the integral (8) in frequency domain.

4 Kirchhoff Simulation

4.1 Derivation

Using the Born approximation, the first order perturbation of $G_F(x_r, z_r, t; x_s, z_s)$ resulting from the perturbation δv of v is given by

$$\begin{aligned}
\delta G_F(x_r, z_r, t; x_s, z_s) \ &= \ \int_{-\infty}^{\infty} dx \int_{z_d}^{\infty} dz \ \left[\frac{2r(x,z)}{v(x,z)^2}\right] \ \frac{\partial^2}{\partial t^2} G_F(x, z, t; x_s, z_s) * \\
&\quad G_F(x, z, t; x_r, z_r) \ ,
\end{aligned} \tag{14}$$

where (x_s, z_s) and (x_r, z_r) are the source and receiver positions, respectively, $z_r, z_s < z_d$. Recall that for a general source $f(t)$, the perturbed solution is given by $\delta p = f * \delta G_F$.

Combination of equations (13) and (4) gives the following asymptotic approximation for G_F

$$G_F(x, z, t; x_p, z_p) \approx \mathcal{G}_{-1}^p(x, z, t) - \mathcal{G}_1^p(x, z, t) \ , \tag{15}$$

where

$$\mathcal{G}_\nu^p(x, z, t) = \frac{(z_d + \nu z_p) \ a_\nu^p(x, z)}{\sqrt{v_0 \ \beta_\nu^p(x, z)} \ R_\nu^p(x, z)^{3/2}} \ \mu(t - t_\nu^p(x, z)) \ ,$$

$$\beta_\nu^p(x, z) = \frac{d^2}{dy^2} \left[\frac{1}{v_0}\sqrt{(y - x_p)^2 + (z_d + \nu z_p)^2} + \tau(y, z_d; x, z)\right]_{y = \alpha_\nu^p(x, z)} \ ,$$

$$R_\nu^p(x,z) = \sqrt{(\alpha_\nu^p(x,z) - x_p)^2 + (z_d + \nu z_p)^2} \,,$$

$$a_\nu^p(x,z) = a(\alpha_\nu^p(x,z), z_d; x, z) \,,$$

$$t_\nu^p(x,z) = \frac{R_\nu^p(x,z)}{v_0} + \tau(\alpha_\nu^p(x,z), z_d; x, z) \,,$$

and

$$\alpha_\nu^p(x,z) = \arg\min_y \left\{ \frac{1}{v_0}\sqrt{(y - x_p)^2 + (z_d + \nu z_p)^2} + \tau(y, z_d; x, z) \right\} \,,$$

for $p \in \{s, r\}$ and $\nu \in \{-1, 1\}$. Note that since x_s, z_s, x_r and z_r are fixed, we dropped them from the parameters of $\mathcal{G}$.
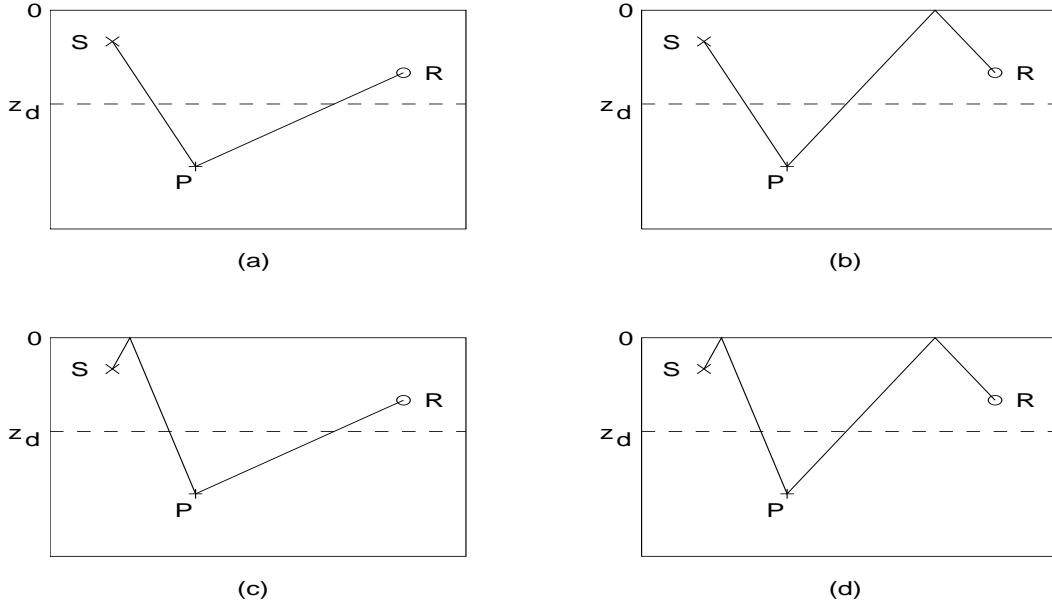
Figure 3: Geometrical representation of the four terms in equation (16). $S = (x_s, z_s)$, $R = (x_r, z_r)$ and $P = (x, z)$. (a) $\eta = \xi = -1$; (b)$\eta = -1$, $\xi = 1$; (c) $\eta = 1$, $\xi = -1$; (d) $\eta = \xi = 1$.

Replacing G_F in equation (14) by the approximation (15), evaluating the convolution, and using the fact that $u * v'' = (u * v')'$, we find the asymptotic formula for δG_F

$$\delta G_F(x_r, z_r, t; x_s, z_s) \approx$$
$$\frac{\partial}{\partial t}\frac{2\pi}{v_0} \sum_{\eta,\xi\in\{-1,1\}} \int_{-\infty}^{\infty} dx \int_{z_d}^{\infty} dz \, \frac{r(x,z)}{v(x,z)^2} \, A_{\eta,\xi}(x,z) \, \delta(t - t_\eta^r(x,z) - t_\xi^s(x,z)) \,, \tag{16}$$

where

$$A_{\eta,\xi}(x,z) = \frac{\eta\xi \, (z_d + \eta z_s)(z_d + \xi z_r) \, a_\eta^s(x,z) a_\xi^r(x,z)}{R_\eta^s(x,z)^{3/2} R_\xi^r(x,z)^{3/2} \beta_\eta^s(x,z)^{1/2} \beta_\xi^r(x,z)^{1/2}} \; .$$

Observe that the first term of the sum in equation (16), corresponding to $\eta = \xi = -1$, gives the perturbed solution without surface reflections, i.e. $\delta G(x_r, z_r, t; x_s, z_s)$ (see Figure 3). Also notice that to compute $\delta p = f * \delta G_F$ we only need to change the function δ in equation (16) to f.

4.2 Computation of $\alpha_\nu^p(x,z)$, $t_\nu^p(x,z)$, $a_\nu^p(x,z)$ and $\beta_\nu^p(x,z)$

The data are the traveltimes and amplitudes for G, recorded at $z = z_d$ and $x_n^d = x_{min}^d + (n-1)\Delta x^d$, $n = 1, \ldots, N_d$: $\tau_n = \tau(x_n^d, z_d; x, z)$ and $a_n = a(x_n^d, z_d; x, z)$, respectively.

Let $\tilde{\tau}(y, z_d; x, z)$ be a procedure that interpolates the value of the traveltimes $\tau(y, z_d; x, z)$ using the values of τ_n, and $\tilde{a}(y, z_d; x, z)$ the analogous procedure for the amplitudes.

Let ℓ be the index such that the traveltime

$$\frac{1}{v_0}\sqrt{(x_\ell^d - x_p)^2 + (z_d + \nu z_p)^2} + \tau(x_\ell^d, z_d; x, z)$$

is minimal. Define the discrete set $Y = \{x_\ell^d + i \, \Delta x^d/N \mid i = -N, \ldots, N\}$ where N is a fixed positive integer (for $\ell = 1$ we start at $i = 0$ and for $\ell = N_d$ we stop at $i = 0$). Therefore, $\alpha_\nu^p(x,z)$ can be approximated by the solution of the following discrete minimization problem

$$\alpha_\nu^p(x,z) \approx \arg\min_{y \in Y} \left\{ \frac{1}{v_0}\sqrt{(y - x_p)^2 + (z_d + \nu z_p)^2} + \tilde{\tau}(y, z_d; x, z) \right\} \; .$$

As a result,

$$t_\nu^p(x,z) \approx \frac{1}{v_0}\sqrt{(\alpha_\nu^p(x,z) - x_p)^2 + (z_d + \nu z_p)^2} + \tilde{\tau}(\alpha_\nu^p(x,z), z_d; x, z)$$

and

$$a_\nu^p(x,z) \approx \tilde{a}(\alpha_\nu^p(x,z), z_d; x, z) \; .$$

To compute β_ν^p, the second derivative of $\tau(y, z_d; x, z)$ at the point $y = \alpha_\nu^p(x,z)$ is approximated by quadratic interpolation through the points $x_{\ell-1}^d$, x_ℓ^d and $x_{\ell+1}^d$ (for $\ell = 1$

we use x_1^d, x_2^d and x_3^d and for $\ell = N_d$ we use $x_{N_d-2}^d$, $x_{N_d-1}^d$ and $x_{N_d}^d$). Therefore,

$$\beta_\nu^p(x,z) \approx \frac{(z_d + \nu z_p)^2}{v_0 \left[(\alpha_\nu^p(x,z) - x_p)^2 + (z_d + \nu z_p)^2\right]^{3/2}} + \frac{\tau_{\ell+1} - 2\tau_\ell + \tau_{\ell-1}}{(\Delta x^d)^2} \ .$$

4.3   Discretization and Algorithm

We introduce the total traveltime field

$$\Psi_{\eta,\xi}(x,z) = t_\eta^r(x,z) + t_\xi^s(x,z) \ .$$

Assume that all grids are uniform. Write $x_k = x_{min} + (k-1)\Delta x$, $z_l = z_{min} + (l-1)\Delta z$ and $t_j = t_{min} + (j-1)\Delta t$, $k, l, j \geq 1$.

Approximating the δ-function by

$$\delta(t) \approx \begin{cases} (\Delta t + t)/\Delta t^2 & , \quad -\Delta t \leq t \leq 0 \\ (\Delta t - t)/\Delta t^2 & , \quad 0 \leq t \leq \Delta t \\ 0 & , \quad \text{otherwise} \end{cases} \ ,$$

(equivalent to perform linear interpolation on f when computing δp) and assuming that $r(x,z)$ vanishes near the edges of the xz-grid, the trapezoidal rule applied to the integrals in equation (16) takes the form:

$$\mathcal{I}_{\eta,\xi}(t_j) = \frac{\Delta x \Delta z}{\Delta t} \sum_{k,l} \frac{r(x_k, z_l)}{v(x_k, z_l)^2} A_{\eta,\xi}(x_k, z_l) \left[(1 - S_{k,l}^{\eta,\xi}) \delta_{j - J_{k,l}^{\eta,\xi} - 1} + S_{k,l}^{\eta,\xi} \delta_{j - J_{k,l}^{\eta,\xi} - 2}\right] \ , \quad (17)$$

where

$$J_{k,l}^{\eta,\xi} = \text{Int}\left(\frac{\Psi_{\eta,\xi}(x_k, z_l) - t_{min}}{\Delta t}\right) \ ,$$

$$S_{k,l}^{\eta,\xi} = \frac{\Psi_{\eta,\xi}(x_k, z_l) - t_{min}}{\Delta t} - J_{k,l}^{\eta,\xi} \ ,$$

$$\delta_j = \begin{cases} 1 & , \quad j = 0 \\ 0 & , \quad j \neq 0 \end{cases} \ ,$$

and $\text{Int}(q)$ denotes the integer part of q.

Finally, the time derivative is approximated by the central-difference formula:

$$\frac{d}{dt} U(t_j) \approx \frac{U(t_{j+1}) - U(t_{j-1})}{2\Delta t} \ .$$

Algorithm. Given x_r, z_r, x_s, z_s and f:

· Precompute the scaling field: $F = \dfrac{2\,\pi\,\Delta x\,\Delta z}{v_0\,\Delta t}$.

· For each k,l (depth point):

   · Define $\tilde{r} = r(x_k, z_l)$ and $\tilde{v} = v(x_k, z_l)$.

   · For each η, ξ (primary index):

      · Calculate a_η^s, a_ξ^r, β_η^s, β_ξ^r, t_η^s, t_ξ^r, R_η^s and R_ξ^r.

      · Calculate $\tilde{A} = A_{\eta,\xi}(x_k, z_l)$.

      · Calculate $J_{k,l}^{\eta,\xi}$ and $S_{k,l}^{\eta,\xi}$.

      · Compute $U = \dfrac{\tilde{r}\,\tilde{A}}{\tilde{v}^2}$.

      · Add to output sample $J_{k,l}^{\eta,\xi} + 1$ the quantity $(1 - S_{k,l}^{\eta,\xi})U$.

      · Add to output sample $J_{k,l}^{\eta,\xi} + 2$ the quantity $S_{k,l}^{\eta,\xi}U$.

· Multiply the output trace by F.

· Apply centered time difference operator to the output trace.

· Convolve the output trace with the source f.

The procedure is repeated for all requested source and receiver positions.

5   Numerical Results

In order to analyze the accuracy of the new approach, we first applied the algorithm presented in the previous section to a homogeneous model, where the traveltimes and amplitudes required by the method can be computed analytically. The velocity is $1.5m/ms$ and the reflectivity is layered as shown in Figure 4. The grid on which velocity and reflectivity fields are defined has spacings $\Delta x = \Delta z = 2m$. Shot depth is $8m$ located at $1600m$ from the left edge of the model. Receivers depth is $12m$ with spacing $24m$, far offset $864m$ and 34 traces per shot gather. The energy source is a Ricker wavelet with peak frequency $30Hz$, and then $z_s \approx 0.4$ wavelengths and $z_r \approx 0.6$ wavelengths.

The amplitudes and traveltimes for the Kirchhoff algorithm were computed exactly at $N_d = 45$ points with $\Delta x_d = 25m$ on the datum depth $z_d = 16m$. We use quadratic

interpolation to approximate the traveltimes and amplitudes on z_d, and $N = 10$ in the minimization step. We test our algorithm for two different grids: $\Delta x = \Delta z = 8m$ and $\Delta x = \Delta z = 4m$. For reference, we simulate the same experiment using a finite-difference scheme of order 2–4 for the linearized acoustic wave equation [6], using a grid with $\Delta x = \Delta z = 2m$ (10 points/wavelength) and $\Delta t = 0.5ms$ to ensure accurate results.
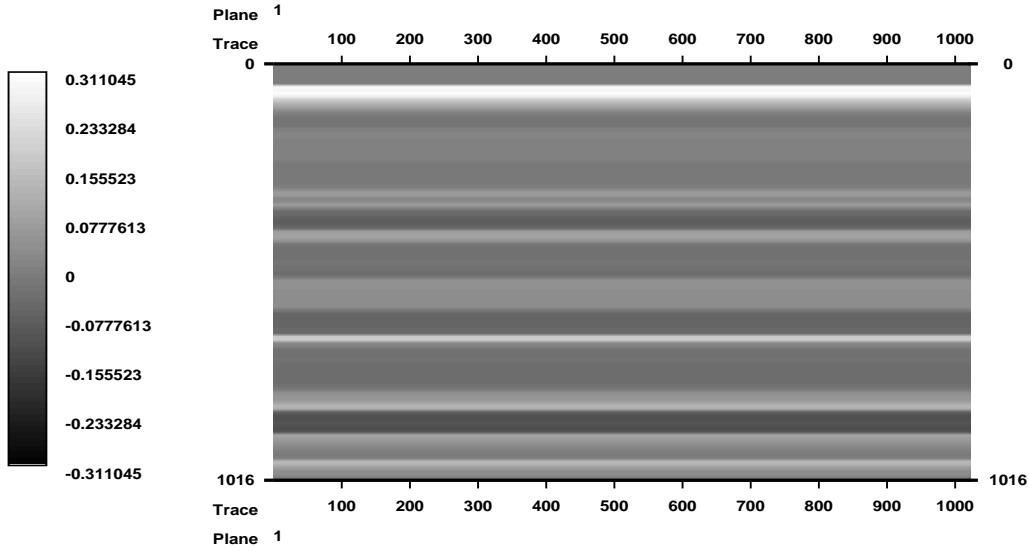

Figure 4: Reflectivity profile for the homogeneous model. Depth axis is in meters.

Figure 5 shows the resulting Kirchhoff simulation for the $8m$ grid and Figure 6 for the $4m$ grid, together with the finite–difference solution and the difference between them. In both cases we use $\Delta t = 0.5ms$. We also made experiments increasing the number of points and/or the size of the datum depth on $z = z_d$, but the results yielded less than 0.5% change in the output.

To show that the approximation for the free–surface Green's function given by equation (2) is not accurate in this case, we show in Figure 7 the resulting Kirchhoff simulation with the derivative approximation on the $4m$ grid. The relative errors in the L_2–norm for the Kirchhoff seismogram in Figure 5.3 are between 4% and 12%, whereas in Figure 5.4 they are between 20% and 121%.
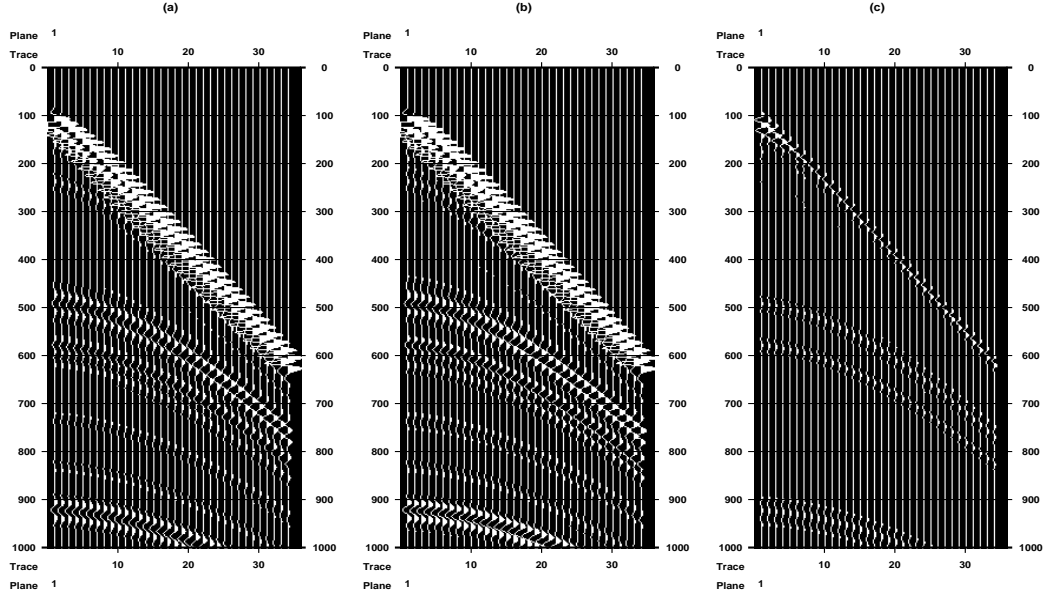
Figure 5: Homogeneous model: $30Hz$ Ricker source wavelet and $\Delta t = 0.5ms$. (a) Finite Differences with $\Delta x = \Delta z = 2m$; (b) Kirchhoff with $\Delta x = \Delta z = 8m$; (c) Difference.
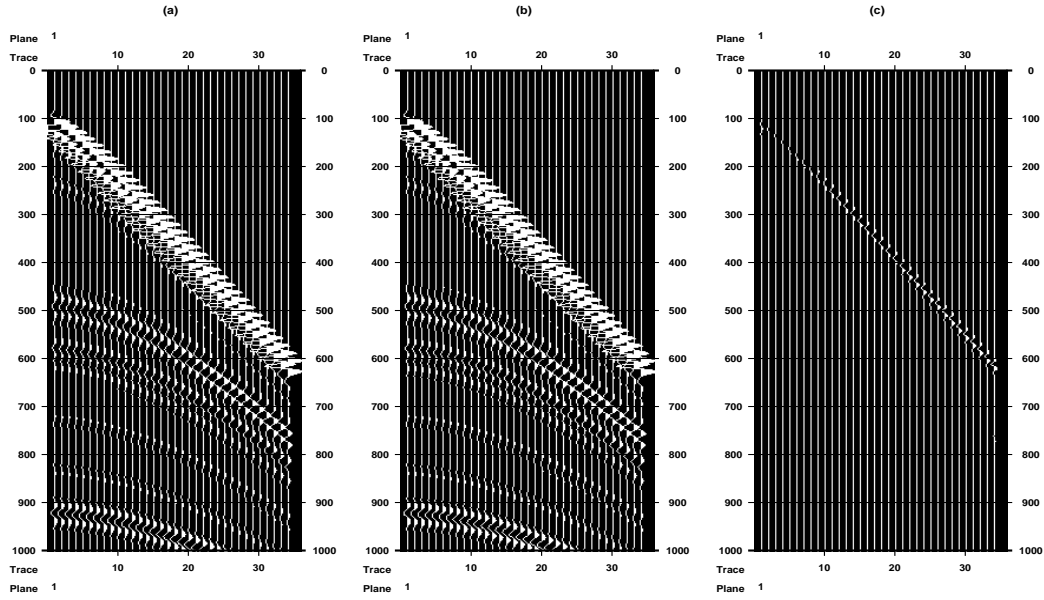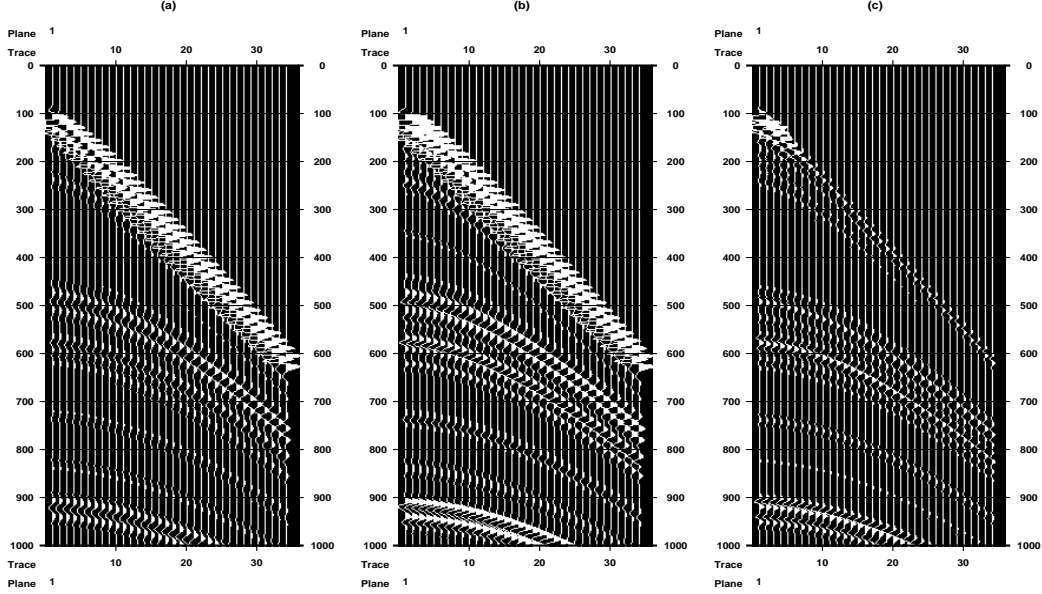

Figure 6: Homogeneous model: $30Hz$ Ricker source wavelet and $\Delta t = 0.5ms$. (a) Finite Differences with $\Delta x = \Delta z = 2m$; (b) Kirchhoff with $\Delta x = \Delta z = 4m$; (c) Difference.

Figure 7: Homogeneous model: $30Hz$ Ricker source wavelet and $\Delta t = 0.5ms$. (a) Finite Differences with $\Delta x = \Delta z = 2m$; (b) Kirchhoff using the approximation (2) for G_F and $\Delta x = \Delta z = 4m$; (c) Difference.

The second model used has the same size and grids of the previous one. The velocity field is almost layered with a slow anomaly embedded in the center, as shown in Figure 8, and the reflectivity is again layered (Figure 9).

Figure 10 shows the resulting Kirchhoff simulation with $\Delta x = \Delta z = 4m$ and $\Delta t = 0.5ms$ for the same source/receiver/datum–depth geometry as in the first model, together with solution produced by the finite–difference code using $\Delta x = \Delta z = 2m$, and the difference between both solutions.The traveltime/amplitude tables were computed using the scheme proposed in [6], which allows the computations being first made in a coarse grid (in this case $8m$) and after interpolated to the original one.
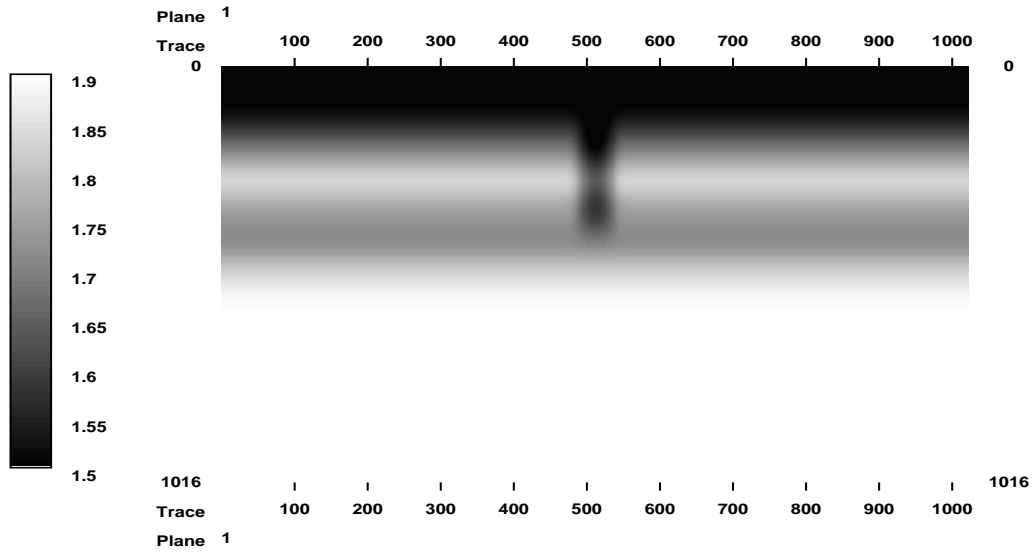
Figure 8: Velocity profile for the nonhomogeneous model. Depth axis is in meters.
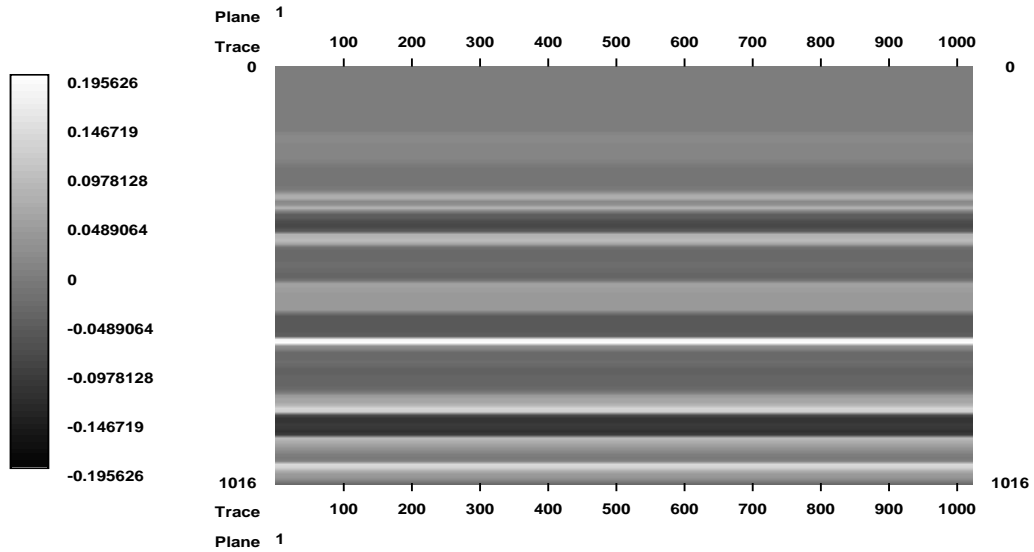

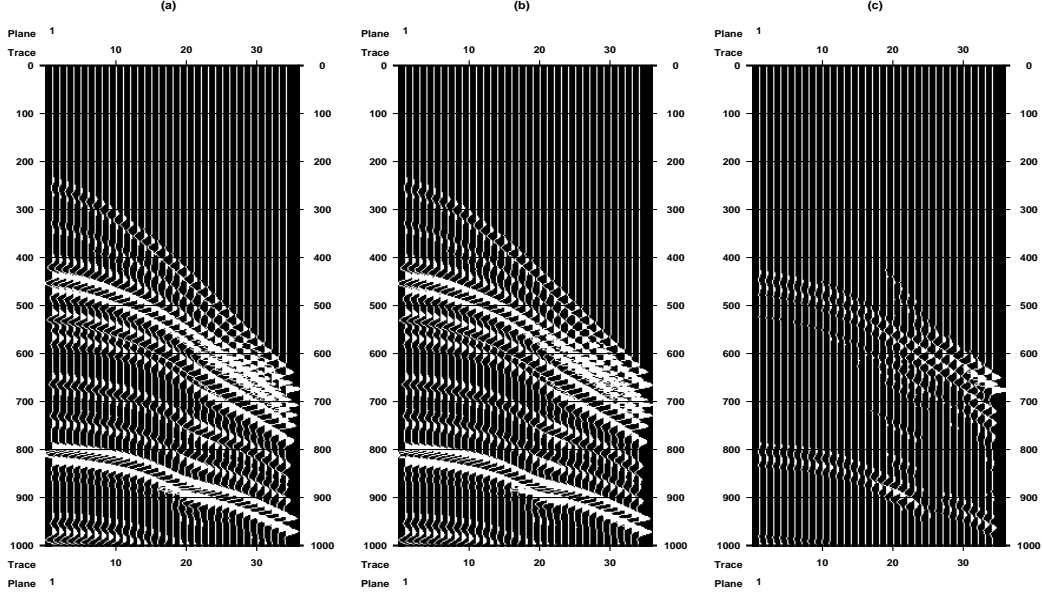Figure 9: Reflectivity profile for the nonhomogeneous model. Depth axis is in meters.

Figure 10: Nonhomogeneous model: $30Hz$ Ricker source wavelet and $\Delta t = 0.5ms$. (a) Finite Differences with $\Delta x = \Delta z = 2m$; (b) Kirchhoff with $\Delta x = \Delta z = 4m$; (c) Difference.

In this experiment the agreement between the seismograms computed by finite differences and Kirchhoff modeling was not as good as in the homogeneous model. This is due to the fact that here the traveltimes are computed by solving the eikonal equation, introducing numerical errors, which also affect the solution of the transport equation for the amplitudes. Moreover, due the slow anomaly in the velocity field the rate of change of traveltimes and amplitudes increases, and so does the truncation error. Nevertheless, we still have reasonable results.

To illustrate the effect of irregular receiver positions, we considered the geometry shown in Figure 11. The resulting Kirchhoff simulation for the $4m$ grid and $\Delta t = 0.5ms$ is shown in Figure 12.
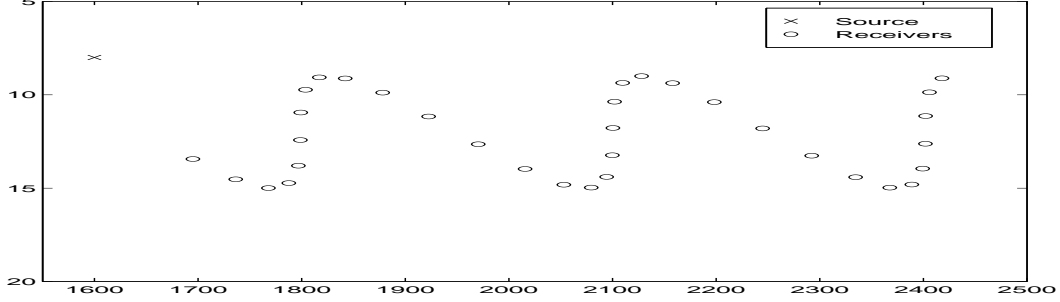
Figure 11: Irregular receiver positions for the nonhomogeneous model. Axes are in meters.
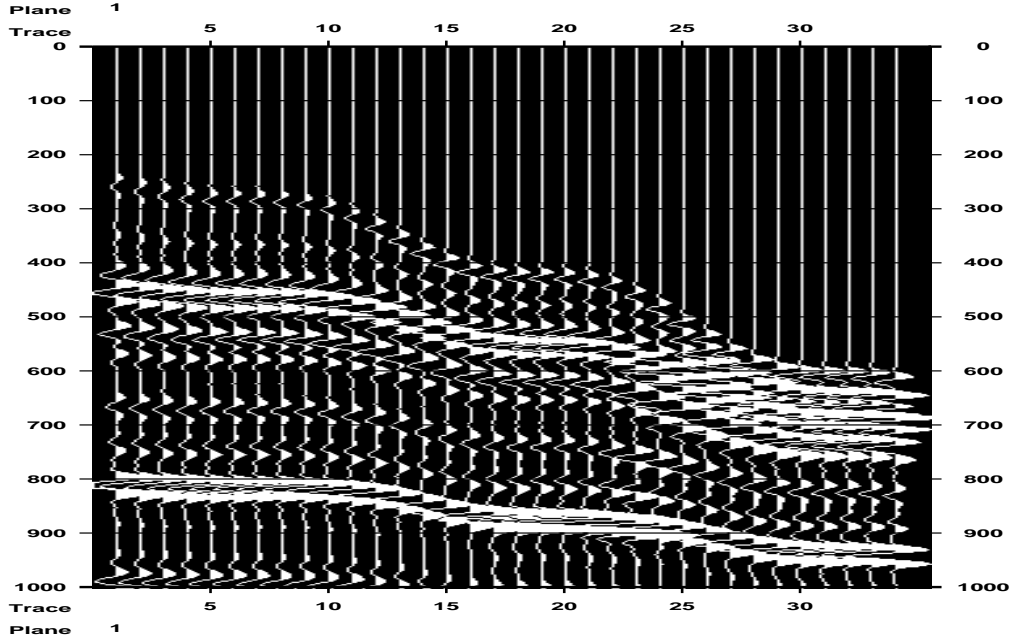

Figure 12: Nonhomogeneous model with irregular receiver positions: $30Hz$ Ricker source wavelet and $\Delta t = 0.5ms$. Kirchhoff simulation with $\Delta x = \Delta z = 4m$.

6   Conclusion

The major cost of usual Kirchhoff simulations lies on the computation of traveltimes and amplitudes, since the Kirchhoff summation itself is quite inexpensive. The new approach presented in this work reduces the cost of such computations. Indeed, once we have com-

puted the traveltimes and amplitudes at the datum depth, we can simulate any experiment with sources and receivers above the datum depth at any place in the domain, even outside the mesh. For irregular source/receiver positions the cost of the introduced scheme is much less expensive than in the usual approach.

From the experiments we can conclude that for the parameter ranges and type of model considered here, primaries only simulation via this new approach for the Kirchhoff modeling also gives accurate results.

Naturally, further significant optimization opportunities are available in the Kirchhoff code. For instance, the scheme to find $\alpha_\nu^p(x, z)$ can be improved. Since the velocity field is smooth, the search for the interval where the signal of the traveltime derivative changes can be done only near the interval founded for the previous depth point.

Another feature of our approach is that the information required from each grid point (traveltimes and amplitudes) can be stored in core, one data set at a time, as we perform the summation for all requested source–receiver positions. This gives an additional improvement on the CPU time, since operations on disk during computation do degrade the performance.

References

[1] R.M. ALFORD, K.R KELLY, D.M. BOORE. Accuracy of Finite Difference Modeling of the Acoustic Wave Equation, *Geophysics*, **39**, 834–842, 1974.

[2] N. BLEISTEIN. Mathematical Methods for Wave Phenomena, Academic Press, 1984.

[3] N. BLEISTEIN. On the Imaging of Reflectors in the Earth, *Geophysics*, **52**, 931–942, 1987.

[4] S.H. GRAY AND W.P. MAY. Kirchhoff Migration Using Eikonal Equation Traveltimes, *Geophysics*, **59**, 810–817, 1994.

[5] A.R. LEVANDER. Fourth Order Finite Difference P-SV Seismograms, *Geophysics*, **53**, 1425–1434, 1988.

[6] W.W. SYMES, R. VERSTEEG, A. SEI AND Q.H. TRAN. Kirchhoff Simulation, Migration, and Inversion using Finite Difference Traveltimes and Amplitudes, *TRIP 94*, Rice University, 1994.

[7] A.N. TIKHONOV AND A.A. SAMARSKII. Equations of Mathematical Physics, Dover Publications, 1963.

[8] A. VAN TRIER AND W.W. SYMES. Upwind Finite–Difference Calculation of Traveltimes, *Geophysics*, **56**, 812–821, 1991.

[9] J. VIDALE. Finite–Difference Calculation of Traveltimes, *Bulletin of the Seismological Society of America*, **78**, 2062–2076, 1988.